J Ginseng Res 41 (2017) 290–297

Contents lists available at ScienceDirect

Journal of Ginseng Research

journal homepage: http://www.ginsengres.org

Research article

Identification of ginseng root using quantitative X-ray microtomography

Linlin Ye [1,☆], Yanling Xue [1,☆], Yudan Wang [1], Juncheng Qi [2], Tiqiao Xiao [1,*]

[1] Shanghai Institute of Applied Physics, Chinese Academy of Sciences, Shanghai, China
[2] School of Information and Communication Engineering, North University of China, Shanxi, China

ARTICLE INFO

Article history:
Received 18 September 2014
Received in Revised form
16 May 2016
Accepted 31 May 2016
Available online 9 June 2016

Keywords:
Panax ginseng
Panax quinquefolius
quantitative microtomography
synchrotron radiation
X-ray phase contrast imaging

ABSTRACT

Background: The use of X-ray phase-contrast microtomography for the investigation of Chinese medicinal materials is advantageous for its nondestructive, *in situ*, and three-dimensional quantitative imaging properties.
Methods: The X-ray phase-contrast microtomography quantitative imaging method was used to investigate the microstructure of ginseng, and the phase-retrieval method is also employed to process the experimental data. Four different ginseng samples were collected and investigated; these were classified according to their species, production area, and sample growth pattern.
Results: The quantitative internal characteristic microstructures of ginseng were extracted successfully. The size and position distributions of the calcium oxalate cluster crystals (COCCs), important secondary metabolites that accumulate in ginseng, are revealed by the three-dimensional quantitative imaging method. The volume and amount of the COCCs in different species of the ginseng are obtained by a quantitative analysis of the three-dimensional microstructures, which shows obvious difference among the four species of ginseng.
Conclusion: This study is the first to provide evidence of the distribution characteristics of COCCs to identify four types of ginseng, with regard to species authentication and age identification, by X-ray phase-contrast microtomography quantitative imaging. This method is also expected to reveal important relationships between COCCs and the occurrence of the effective medicinal components of ginseng.

1. Introduction

As a result of the spatial coherence improvement of X-rays from synchrotron radiation facilities [1,2], the application of X-ray phase-contrast microtomography (XPCMT) as a useful scientific research method has been expanded to the comprehensive study of Chinese medicinal materials (CMMs) to nondestructively investigate the characteristic microstructures of ginseng and evaluate ginseng quality [3,4]. XPCMT has many advantages; for instance, it provides nondestructive, *in situ*, and three-dimensional (3D) quantitative imaging. The current study applied a phase-retrieval process to generate a quantitative image using XPCMT and specifically to identify ginseng.

Ginseng is a slow-growing perennial herbaceous plant as well as a CMM that is well known worldwide. *Panax quinquefolius* L. (American ginseng) and *Panax ginseng* Meyer (Asian ginseng) are the two predominant *Panax* species grown commercially in North America and Asia, respectively [5]. Ginseng is grown for its highly valued root, which plays an important role as a medicinal resource and in nutrition. The major attraction of ginseng is its wide range of pharmacological effects [6–8]. The medicinal value of ginseng is attributed mostly to ginsenosides. The content of ginsenosides varies depending on the light level [9], fertility level [10], plant part, age [11], harvest date [12], and drying condition [13]. In the marketplace, the quality of ginseng root is graded based on several factors, such as species, production area, growth pattern, age grade, and external shape, and these characteristics are closely related to its medicinal value. Currently, ginseng is primarily identified with the naked eye. It is particularly important to judge the growing conditions nondestructively during the quality grading process of ginseng.

* Corresponding author. Shanghai Synchrotron Radiation Facility, Shanghai Institute of Apllied Physics, Chinese Academy of Sciences, 239 Zhangheng Road, Pudong District, Shanghai 201204, China.
E-mail address: tqxiao@sinap.ac.cn (T. Xiao).
☆ These authors contributed equally to this work.

http://dx.doi.org/10.1016/j.jgr.2016.05.004
p1226-8453 e2093-4947/$ – see front matter

With the development of new technologies, both physicochemical and microscopic identification methods have been used in CMM research. Physicochemical methods are well adapted for quantitative research, whereas microscopic identification methods are appropriate for qualitative research. In general, both quantitative and qualitative research methods have been adapted for the authentication, quality assessment, and age assessment of ginseng species. However, only biological and chemical methods can provide accurate data to quantitatively identify and evaluate ginseng [14–17]. Qualitative identifications of CMMs have been performed using imaging techniques by employing light and scanning electron microscopy [18,19]. Sample preparations rely on traditional paraffin sectioning; thus, this technique provides information only about static cross sections, and samples are greatly damaged during this process. Although the traditional slice accumulation method can yield 3D imaging information, the disadvantages of this method are the unavoidable deviations introduced during the process of slicing. Moreover, reconstruction of the 3D appearance of the microstructure from dissection or a sectional series requires particular scientific drawing skills, which are always a matter of the artist's interpretation. This approach also causes wastage of materials, and much time is required for sample preparation. Magnetic resonance imaging leads to low image resolution, and temperature easily influences sample moisture. This irregular moisture distribution makes it more difficult to produce an acceptable magnetic resonance image [20]. Therefore, these methods are not completely suitable for the study of precious samples.

Currently, all the methods discussed above have their new applications; however, these methods are unable to satisfy the demand for nondestructive and *in situ* research. Practical application requires that wild ginseng is left intact; therefore, destructive methods are not suitable for research on highly valuable wild ginseng. Nondestructive research methods for *in situ* ginseng identification continue to rely on the rich experience of prestigious experts who judge its quality based on appearance and other characteristics. Owing to a lack of scientific data, identification by experience occasionally results in errors. Recently, a kind of computed tomography (CT) scanner was used to evaluate ginseng quality via nondestructive inspection of the internal tissue density of ginseng [21]. However, the CT scanner neither achieves independent or effective detection, nor provides high-resolution imaging results. Thus, the CT scanner is unable to provide reliable identification information or to lead to a quantitative analysis. The current study addresses these problems.

Calcium oxalate cluster crystals (COCCs) are a kind of secondary metabolite found in medicinal plants; the shape, distribution, and amount of crystals are important characteristics for microscopic identification of medicinal plants. Accumulation of secondary metabolites in medicinal plant roots is also correlated with plant age [13]. We undertook this study to obtain quantitative information on ginseng microstructures and identify different types of ginseng using XPCMT. The objectives of this study were (1) to report the efficiency of XPCMT with regard to the quantitative identification of ginseng root and (2) to correlate the accumulation characteristics of ginseng COCCs with the identification results of the different types of ginseng.

2. Materials and methods

2.1. Materials

Many investigations on American and Asian ginseng have been published over the past decade [22]. Asian ginseng can be either wild or cultivated. Wild ginseng is classified as a national protected plant of the first class in China. Therefore, not only is wild ginseng rare in CMMs, but its specimens also have an extremely high value to collectors. Samples of Asian and American ginseng were used in this investigation. Cultivated and wild ginseng of the same species, but with different ages and different growth patterns, were selected from the same cultivated area (Changbai Mountain, China). Korean ginseng is cultivated in South Korea, and American ginseng is cultivated in Canada. All these ginsengs were purchased from Beijing Tong Ren Tang. The age of wild ginseng is 26 yr and cultivated ginseng is 6 yr; the Korean ginseng and American ginseng are several years old, but there is no exact age recorded for them. Based on the characteristics of the four samples of raw ginseng root, three different groups were established to distinguish them by their different growing conditions. The major differences were between species (Korean ginseng and American ginseng), ignoring the influence of the different growing areas. In addition to species, the major difference between the samples was the location where they were grown. The main differences between cultivated ginseng and wild ginseng were their age grades and their growing conditions.

2.2. Sample preparation

In contrast with techniques such as scanning electron microscopy and transmission electron microscopy, XPCMT does not require samples to be sliced. Other features of XPCMT are of major interest, such as avoiding time-consuming preparation, reducing chemicals, eliminating the artifacts introduced by different sample preparation procedures, and avoiding internal structural damage to the whole ginseng. However, we must also consider the problem of deformation due to sample shrinkage during XPCMT. Sample deformation directly destabilizes imaging quality and can even prevent the acquisition of experimental data. Sample deformation is caused by the high moisture content that is then heated by X-ray irradiation. Therefore, most of the water must be removed during sample preparation to ensure that the internal structure of the ginseng is not damaged or deformed. The allowed deformation value is $\leq$3.7 μm in every direction of the overall sample tissue. Sample drying should be conducted at a constant temperature and constant humidity. In the current study, all the ginseng samples were dried at a constant temperature (25°C) for 1 month. Studies were conducted on the lower portion of taproot in wild ginseng and on the upper part of the lateral root in the other samples. All sample diameters ranged between 4 mm and 7 mm.

2.3. Methods and experimental setup

As ginseng weakly absorbs X-rays, X-ray absorption imaging is not suitable for such low-*Z* materials. X-ray phase-contrast microscopy is advantageous given its high sensitivity for low-*Z* materials [1,2,23,24]. XPCMT is a highly promising method because of its nondestructiveness, suitability for *in situ* and 3D measurements, and sensitivity for low-*Z* materials [25]. To date, XPCMT has been used successfully for plant research [26–28]. X-ray phase-contrast microscopy has already provided preliminary exploratory results [29,30], and XPCMT has been adapted to study CMM raw materials [3,4]. In this study, XPCMT data processing using the phase-retrieval method was employed to obtain quantitative information about the microstructure of ginseng. We found that XPCMT can be used to identify ginseng.

XPCMT experiments on ginseng were performed at the X-ray imaging and biomedical application beamline (BL13W1) of the Shanghai Synchrotron Radiation Facility in China. The third-generation synchrotron radiation facility provides an excellent X-ray imaging resource with the advantages of monochromaticity, high spatial coherence, and high flux density. The white beam that results from wiggler radiation is monochromatized via a Si(111) and

Si(311) double-crystal monochromator, which enables an X-ray photon output at 8–72.5 keV and energy resolution of approximately 0.5%. An ionization chamber was employed to monitor the flux during the experiments. Entrance and exit slit systems were used to define the input and output beams for the monochromator, and the maximum size of the beam cross section was 45 mm (horizontal) × 5 mm (vertical). The distance between the radiation source and the central point of the sample stage was approximately 34 m. The XPCMT experimental setup, which is identical to that of absorption-based CT except for the increased sample-to-detector distance, is particularly simple and provides a high, spatially coherent beam [31]. A precision multidimensional sample stage with six axes was installed for microtomography. The schematic diagram for the XPCMT experimental system is shown in Fig. 1. XPCMT has a simple experimental design, and it can produce high-resolution imaging results quickly and efficiently.

2.4. Experimental parameters

For an XPCMT experiment, several experimental parameters should be determined and optimized. The optimum energy was chosen to obtain the best image by considering factors such as penetration ability, phase contrast, and detection efficiency. During the experiments, the propagation-based XPCMT protocol was employed, and the optimized sample-to-detector distance was selected to provide highly edge-enhanced X-ray images. A suitable exposure time was selected to ensure a sufficiently high signal-to-noise ratio. The specific experimental parameters used in the current ginseng research were as follows: the photon energy was set at 14 keV, and the sample-to-detector distance was 10 cm. An Optique Peter X-ray detector was employed, and its effective resolution was 3.7 μm/pixel. When the sample was rotated horizontally, a dataset for the projected images (including sample images from 0° to 180°) was collected. The XPCMT projection number selected for the current research was 1080 based on the sample size and spatial resolution.

2.5. Data processing and analysis

The data reconstruction was related to the 3D Laplacian of the refractive index distribution, which is usually a form of edge-enhancement imaging. Moreover, for the quantitative imaging and analysis, the phase-retrieval method can be coupled to an XPCMT algorithm to resolve the phase-shift problem. The sample induces the phase-shift phenomenon, and the contrast is recorded on an imaging plane [32]. The solution is to first retrieve the phase of each projection. Subsequently, the filtered backprojection algorithm reconstructs the slices [33]. The edge-enhancement effect is faded, and similar components of the microstructure display enhanced gray-level uniformity. The final results can be used for quantitative analysis.

Fig. 2 shows a clear microstructural study of the ginseng root slices. Phase-retrieval imaging of ginseng tissue produces a homogeneous grey level and an optimized view of the internal microstructure of the ginseng root. Ginseng root contains low elements such as C, H, O, and N; however, COCCs contain calcium and have a higher density. Thus, quantitative information concerning the COCCs can be extracted from the rest of the microstructures. The distribution of the COCCs is clearly shown as punctiform highlights in the images. As Fig. 2A shows, the COCC distribution was divided into two parts (IN and OUT) by the cambium structure (CS). According to the position of the CS, the ginseng tissue was divided into two parts, also called “IN” and “OUT”. Both parts of the ginseng tissue contain COCCs; however, the CS tissue does not contain COCCs. Direct observations of the ginseng microstructure using virtual slices revealed that the American ginseng had the least amount of COCCs (see Fig. 2B), with almost no COCCs found in the IN position.

3. Results and discussion

3.1. Quantitative information acquisition

As mentioned above, accumulation of secondary metabolites in medicinal plant roots is correlated with plant age. Therefore, investigation of the secondary metabolite accumulation to determine the age of herbal plant roots is important in root-based medicines. However, unlike wild plants, certain commonly used CMMs were distributed across different climatic zones and altitudes after they were first introduced; furthermore, their cultivation methods differ. These conditions make determining the medicinal value of certain perennial herbs more complex. However, plant tissue contains different types of crystalline materials. As each type of plant crystal has a stable composition and form, different crystal forms as well as their size and distribution can be used to identify plant species. The microstructure of crystals in plants provides important evidence to identify CMM species and attempt to classify unknown CMMs. COCC is an important secondary metabolite in ginseng. XPCMT and the phase-retrieval method extracted quantitative information regarding ginseng COCCs. COCC information is useful because it provides different characteristics to compare the four types of ginseng root used in our research: cultivated ginseng, American ginseng, Korean ginseng, and wild ginseng. The results show that XPCMT can be used to identify different types of ginseng. Clear and detailed results follow.

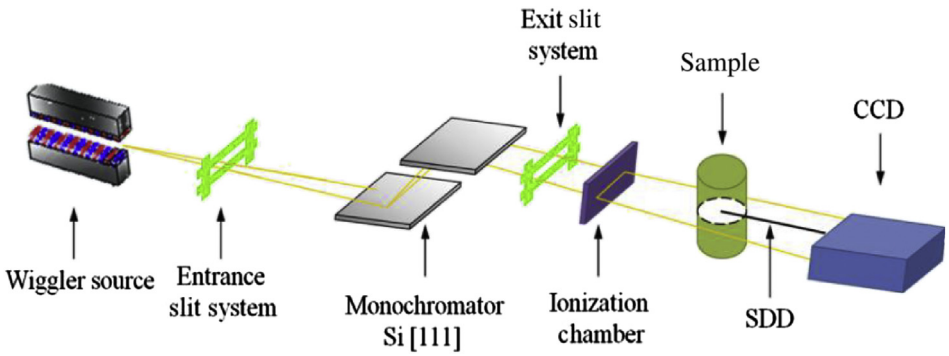

Fig. 1. A schematic diagram of the XPCMT system. CCD: charge-coupled device; SDD, sample-to-detector distance; XPCMT, X-ray phase-contrast microtomography.

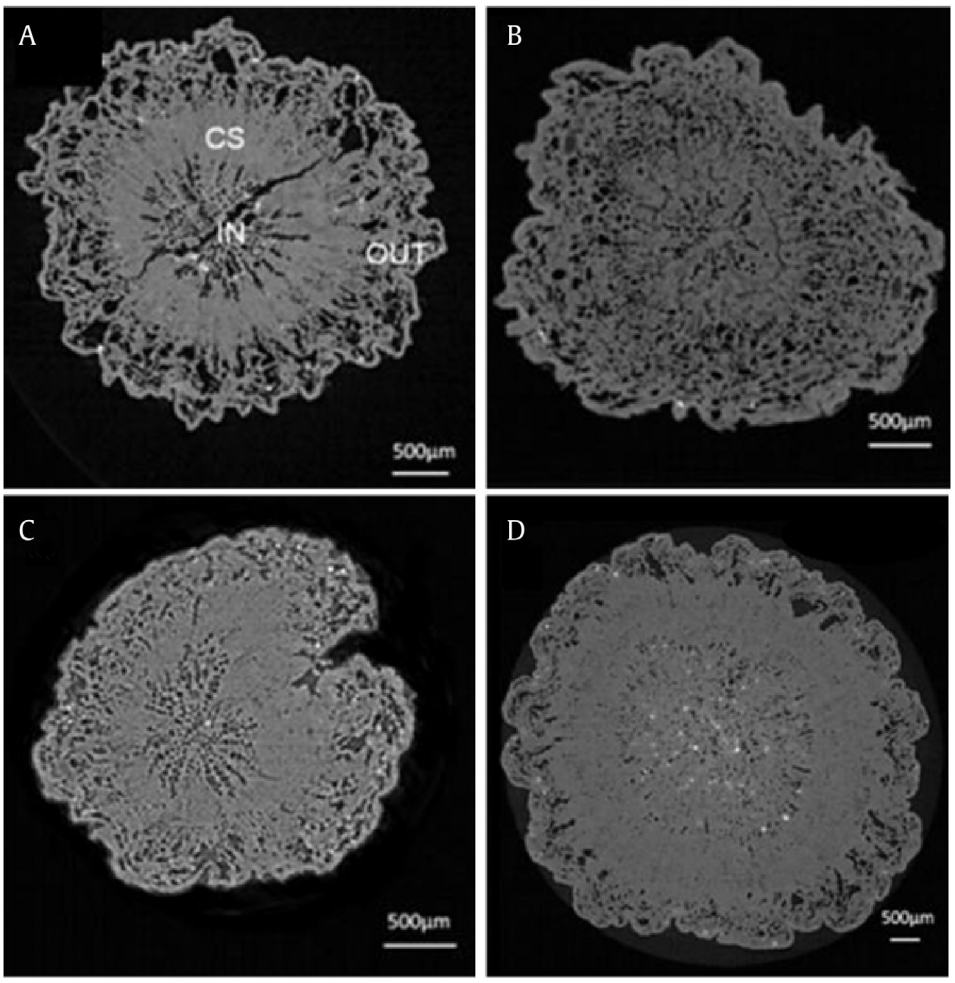

Fig. 2. Cross sections of ginseng root. XPCMT slices of (A) cultivated ginseng, (B) American ginseng, (C) Korean ginseng, and (D) wild ginseng. CS, cambium structure; IN, ginseng tissue inside the cambium structure; OUT, ginseng tissue outside the cambium structure; XPCMT, X-ray phase-contrast microtomography.

The results clearly revealed the microstructures of ginseng and proved that XPCMT can provide quantitative information for the microscopic identification of ginseng. The characteristics of COCCs are different from those of their surrounding tissues in ginseng. Therefore, the phase-retrieval method is appropriate for extracting quantitative information regarding COCCs. We observed additional virtual slices and created 3D images of COCCs for 100 slices with a thickness of 370 μm. The 3D quantitative imaging results were sufficient for all statistical analyses, including the distribution of COCC volume as well as the amount of COCCs and their morphological distribution. Based on the 3D quantitative results, COCCs are easy to separate and extract from ginseng tissues.

3.2. Quantitative analysis of COCCs

The current study emphasized the discussion on the distribution characteristics of ginseng COCCs. We found that the COCC distribution data can provide evidence to identify the four types of ginseng.

3.2.1. Species identification from 3D imaging results

First, we obtained 3D results for the COCC distribution using 370-μm-thick ginseng tissue (as shown in Fig. 3). We found only a few (approx. 3–5) COCCs in the "IN" portion of American ginseng and apparently much more in the other three samples. Wild and Korean ginseng had numerous COCCs. Therefore, we can preliminarily differentiate between American ginseng and other types of ginseng based on the amount and distribution of COCCs.

3.2.2. Ginseng COCC quantitative data

The COCCs of ginseng were quantitatively analyzed. The total number of COCCs is shown in Fig. 4A, and its calculation method is provided in Eq. (1):

$$SN_j = \sum num_j(Ai) \quad (1)$$

where $i \in \{1, 2, \ldots, 8\}$, $j \in \{1, 2, 3, 4\}$ ($j = 1$, cultivated ginseng; $j = 2$, American ginseng; $j = 3$, Korean ginseng; and $j = 4$, wild ginseng); SN_j is the number of COCCs; and $num_j(Ai)$ is the count of COCCs in the range of A*i*. A*i* is the value set for all COCC volumes and was derived from the volume of a single particle of COCC. Group A1 ($i = 1$) consisted of a COCC volume less than 1,000 μm^3, and the remaining COCCs are classified as shown in Table 1.

A graph of the analysis of the total volume of COCCs is shown in Fig. 4B, and the calculation method is provided in Eq. (2):

$$SV_j = \sum vol_j(Ai) \quad (2)$$

where $i \in \{1, 2, \ldots, 8\}$, $j \in \{1, 2, 3, 4\}$ ($j = 1$, cultivated ginseng; $j = 2$, American ginseng; $j = 3$, Korean ginseng; and $j = 4$, wild ginseng);

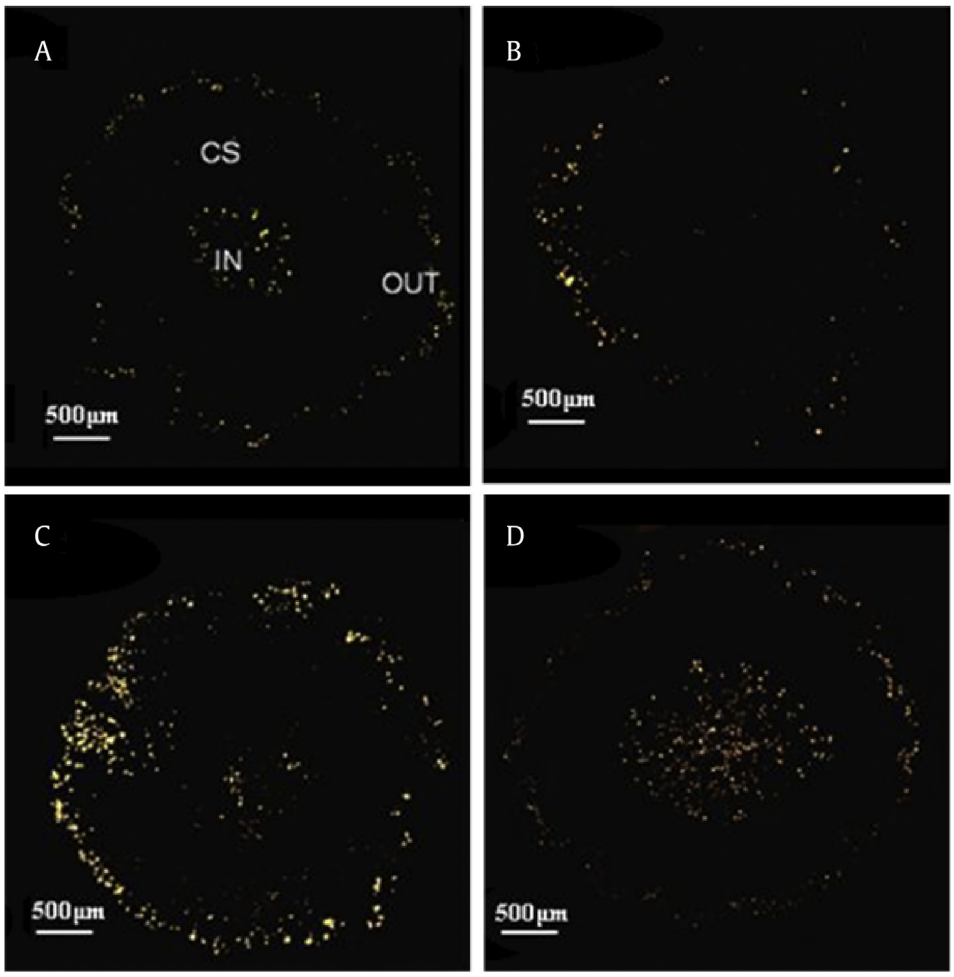

Fig. 3. Distribution of COCCs. COCC distribution position in (A) cultivated ginseng, (B) American ginseng, (C) Korean ginseng, and (D) wild ginseng. COCC, calcium oxalate cluster crystal; CS, cambium structure; IN, ginseng tissue inside the cambium structure; OUT, ginseng tissue outside the cambium structure.

SV_j is the COCC total volume; and $vol_j(Ai)$ is the volume of COCCs in the range of *Ai*.

As Fig. 4A shows, the number of COCCs in wild ginseng was almost twice that in cultivated ginseng. Of the four types of ginseng, the wild ginseng sample was the oldest one; it is marked as 26 yr old by the certification of quality authentication. As COCC is a secondary metabolite of ginseng, it accumulates with age. A relationship exists between ginseng age and the number of COCCs. The positive relationship with regard to the degree of COCC accumulation can be expressed by the changes in number and volume. Therefore, older ginseng will have a greater degree of accumulation of COCCs. Cultivated ginseng and wild ginseng are the same species and grown in the same areas, but they are of different ages; therefore, the number and volume of the COCCs enable a direct estimation of ginseng age (as shown in Figs. 4A and 4B).

Although cultivated ginseng, Korean ginseng, and American ginseng were of a similar age (approx. 5–6 yr old), the number of Korean ginseng COCCs was relatively high, which indicates that the major influencing factor was the area of growth. Conversely, American ginseng had the lowest amount of COCCs, in terms of

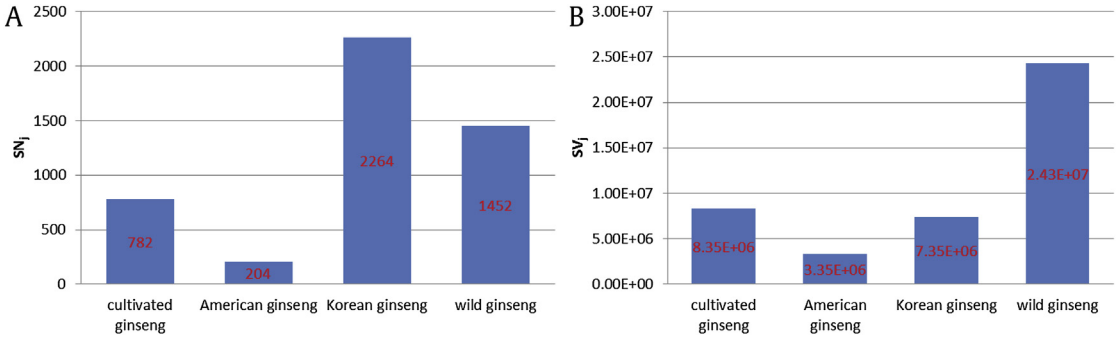

Fig. 4. Quantitative analysis of COCCs in ginseng. (A) Total number and (B) volume of COCCs in four kinds of ginseng of 370 μm thickness. COCC, calcium oxalate cluster crystal.

Table 1
Group range classification according to the different volumes of COCCs

Group	A1	A2	A3	A4	A5	A6	A7	A8
Range (μm^3)	<1,000	1,000–2,000	2,000–5,000	5,000–10,000	10,000–20,000	20,000–50,000	50,000–100,000	>100,000

COCC, calcium oxalate cluster crystal.

both total number and total volume. In this case, species was the primary influencing factor. Therefore, American ginseng has clearly different COCC distribution characteristics (as shown in Fig. 3), and the study of COCCs provides evidence that can identify the American ginseng species.

Wild ginseng had fewer individual COCCs (Fig. 4A), but a higher total volume of COCCs than Korean ginseng (Fig. 4B). The reason for this finding is that the majority of individual COCCs in wild ginseng had a higher volume than individual COCCs in Korean ginseng. The fact that Korean ginseng and cultivated ginseng have similar total volumes of COCCs might be related to their similar ages. We found that the majority of individual COCCs had greater volumes in cultivated ginseng than in Korean ginseng.

3.3. Statistical analyses of ginseng COCCs

3.3.1. Full study of ginseng COCCs

Accurate statistical calculations can provide exact results for ginseng identification. Fig. 5A shows the graph of the percentage of COCCs, and Eq. (3) provides the calculation method:

$$PN_j(Ai) = num_j(Ai)/SN_j \times 100\% \quad (3)$$

where $i \in \{1, 2,\ldots, 8\}$, $j \in \{1, 2, 3, 4\}$ ($j = 1$, cultivated ginseng; $j = 2$, American ginseng; $j = 3$, Korean ginseng; and $j = 4$, wild ginseng); $PN_j(Ai)$ is the percentage of the COCC distribution in different volume ranges of A*i*.

As Fig. 5A shows, American ginseng $PN_2(Ai)$ and wild ginseng $PN_4(Ai)$ had the same distribution tendencies. The difference between these ginseng types is that the wild ginseng $PN_4(Ai)$ curve changes more gently in the range of A3–A6. The percentage of COCCs of Korean ginseng [$PN_3(Ai)$] decreased, which was completely different from those of the other samples. We showed that Korean ginseng's percentage of COCCs was primarily distributed in the range of A1–A3; therefore, the characteristic curve for this feature can differentiate Korean ginseng from other species. A common characteristic of the four ginseng samples was a small proportion in the range of A7 and A8 (as shown in Fig. 5A).

Fig. 5B shows the graph of the percentage of COCC volume, and Eq. (4) provides the calculation method:

$$PV_j(Ai) = vol_j(Ai)/SV_j \times 100\% \quad (4)$$

where $i \in \{1, 2,\ldots, 8\}$, $j \in \{1, 2, 3, 4\}$ ($j = 1$, cultivated ginseng; $j = 2$, American ginseng; $j = 3$, Korean ginseng; and $j = 4$, wild ginseng), and $PV_j(Ai)$ is the percentage of COCC volume distribution across different volume ranges of A*i*.

As is shown in Fig. 5B, cultivated ginseng, American ginseng, and wild ginseng have similar COCC volume percentage distribution curves. In particular, cultivated ginseng and wild ginseng have almost consistent distribution tendencies and proportions, whereas American ginseng has a bit larger full-width at half-maximum value. The $PV_j(Ai)$ of wild ginseng and that of cultivated ginseng indicate that the same species and same growth areas are important factors that affect the curve tendency. Korean ginseng has a completely different volume percentage distribution curve from the others, which provides evidence that can identify Korean ginseng based on its different growth area. Fig. 5B shows the common characteristic of the point A6, which had the maximum volume percentage value for all four types of ginseng.

The total volume of ginseng tissue was denoted as $TVOL_j$, and the subsection volume density distribution of COCCs was $svd_j(Ai)$.

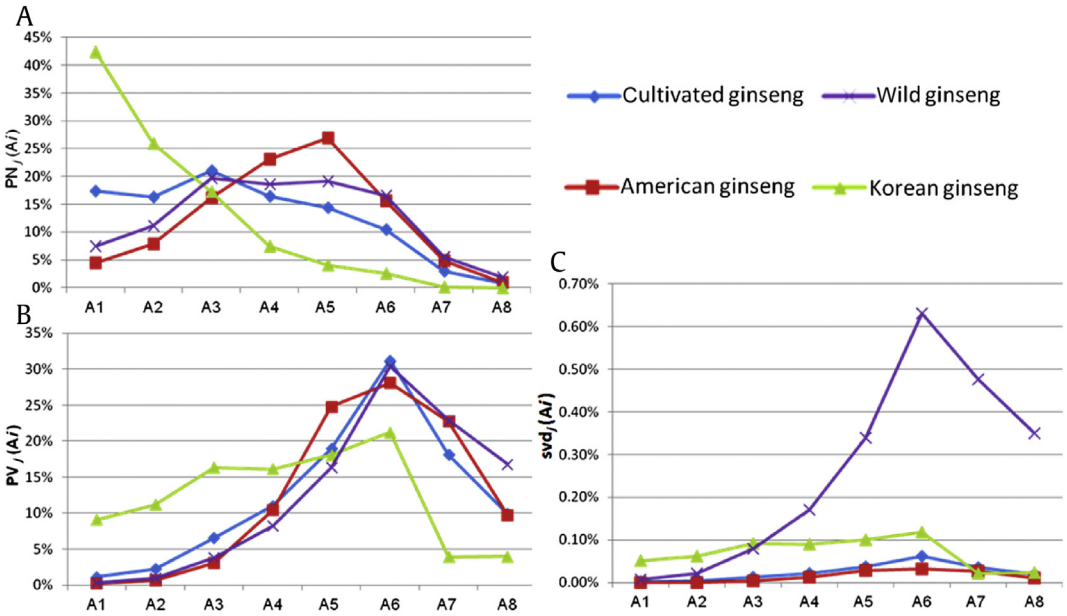

Fig. 5. COCC distribution curves of four different ginseng types. (A) COCC number percentage distribution PN*j*(A*i*), (B) COCC volume percentage distribution PV*j*(A*i*), and (C) COCC subsection volume density distribution in volume range A*i*. COCC, calcium oxalate cluster crystal.

Fig. 5C shows the graph for $svd_j(Ai)$, and Eq. (5) provides the calculation method:

$$svd_j(Ai) = vol_j(Ai)/TVOL_j \times 100\% \quad (5)$$

where $i \in \{1, 2,\ldots, 8\}$, $j \in \{1, 2, 3, 4\}$ ($j = 1$, cultivated ginseng; $j = 2$, American ginseng; $j = 3$, Korean ginseng; and $j = 4$, wild ginseng).

Wild ginseng has the highest value of $svd_4(Ai)$, which ranges from A4 to A8. Cultivated ginseng and American ginseng have similar COCC densities; these results are shown by the $svd_1(Ai)$ and $svd_2(Ai)$ curves. Korean ginseng has a unique COCC density tendency, as shown in Fig. 5C; $svd_3(Ai)$ value was higher than $svd_1(Ai)$ and $svd_2(Ai)$ values for $i = \{1, 2,\ldots, 6\}$.

3.3.2. Disassembly study of ginseng COCCs

All four types of sample tissue were subdivided into two parts: IN and OUT (see Figs. 2 and 3). Statistical and comparative analyses were conducted for the COCC number and volume distribution characteristics of the IN and OUT parts.

The data of each sample were dealt with in two parts: the IN and OUT parts. $PN_{jIN}(Ai)$ is the percentage of the COCC distribution for the IN part across volume ranges of A*i*. Fig. 6A shows the graph of $PN_{jIN}(Ai)$, and Eq. (6) shows the calculation method. SN_j is the total COCC, and $num_{jIN}(Ai)$ is the count of COCCs in the range of A*i* within the IN part. $PN_{jOUT}(Ai)$ is the percentage of the COCC distribution in the OUT part. $Num_{jOUT}(Ai)$ is the count of COCCs in the range of A*i* in the OUT part. Fig. 6A shows the graph of $PN_{jOUT}(Ai)$, and Eq. (7) shows the calculation method:

$$PN_{jIN}(Ai) = num_{jIN}(Ai)/SN_j \times 100\% \quad (6)$$

$$PN_{jOUT}(Ai) = num_{jOUT}(Ai)/SN_j \times 100\% \quad (7)$$

where $i \in \{1, 2,\ldots, 8\}$, $j \in \{1, 2, 3, 4\}$ ($j = 1$, cultivated ginseng; $j = 2$, American ginseng; $j = 3$, Korean ginseng; and $j = 4$, wild ginseng).

Fig. 6A shows interesting results: $PN_{4IN}(Ai) < PN_{4OUT}(Ai)$, $i = \{1, 2, 3, 4\}$, and $PN_{4IN}(Ai) > PN_{4OUT}(Ai)$, $i \in \{5, 6, 7, 8\}$. There is a slight difference in the percentage of the wild ginseng COCC distribution between the IN and OUT parts, just as the corresponding curves shown in Fig. 6A, and A4 and A5 marked the boundary values of transformation. The percentage distributions for the other three samples, between the IN and OUT parts, did not indicate a curve tendency similar to that of wild ginseng (see Fig. 6A). The percentage curve of American ginseng in the OUT part, $PN_{2OUT}(Ai)$, shows an exceptional tendency similar to a Gaussian distribution curve, and the IN part percentage curve, $PN_{2IN}(Ai)$, almost overlaps the horizontal axis, because the percentage value was very low. Both cultivated ginseng and Korean ginseng showed a declining trend. For Korean ginseng, as shown by $PN_{3OUT}(Ai)$ curve in Fig. 6A, the COCCs were mainly distributed in the OUT part in the range of A1–A3. Both the IN percentage curve, $PN_{1IN}(Ai)$, of cultivated ginseng and the $PN_{3IN}(Ai)$ curve of Korean ginseng showed flat trends. Therefore, the key evidence to distinguish cultivated ginseng from Korean ginseng is the COCC percentage value in the OUT part, and the fundamental differences were the values of $PN_{1OUT}(Ai)$ and $PN_{3OUT}(Ai)$, $i = 1, 2$.

As Fig. 6B shows, $PV_{jIN}(Ai)$ and $PV_{jOUT}(Ai)$ are the COCC volume percentage distribution of the IN and OUT parts, respectively, while $vol_{jIN}(Ai)$ and $vol_{jOUT}(Ai)$ are the COCC volumes in the range of A*i* of the IN and OUT parts separately. Fig. 6B shows the curves of $PV_{jIN}(Ai)$ and $PV_{jOUT}(Ai)$, and Eqs. (8) and (9) shows the calculation methods:

$$PV_{jIN}(Ai) = vol_{jIN}(Ai)/SV_j \times 100\% \quad (8)$$

$$PV_{jOUT}(Ai) = vol_{jOUT}(Ai)/SV_j \times 100\% \quad (9)$$

where $i \in \{1, 2,\ldots, 8\}$, $j \in \{1, 2, 3, 4\}$ ($j = 1$, cultivated ginseng; $j = 2$, American ginseng; $j = 3$, Korean ginseng; and $j = 4$, wild ginseng).

As Fig. 6B shows, the COCC volume percentage distributions of the OUT parts of both American and Korean ginseng were much higher than those of the IN part in the range of A4–A8. The IN part COCC volume of wild ginseng was 14,822,986 μm^3, and its OUT part COCC volume was 9,388,866 μm^3; they were relatively closer to each other than to that of other three ginseng, especially in the range of A1–A4, as shown in Fig. 6B. In the range of A4–A8, the wild ginseng volume percentage curve was quite different from that of others because the $PV_{4IN}(Ai)$ volume percentage value of its IN part was higher than that of its OUT part, $PV_{4OUT}(Ai)$. These results indicate that during the early period of ginseng growth, as for the secondary metabolite of COCCs, the OUT part has a faster accumulation speed than the IN part; thus, it showed higher COCC number percentage values and COCC volume percentages values, e.g., $PN_{jOUT}(Ai) > PN_{jIN}(Ai)$ and $PV_{jOUT}(Ai) > PV_{jIN}(Ai)$, $j = 1, 2, 3$; $i \in \{1, 2,\ldots, 8\}$. However, for the more mature ginseng—wild ginseng, the percentage values of the IN and OUT parts approach each other, e.g., $PN_{4OUT}(Ai) < PN_{4IN}(Ai)$, $i \in \{1, 2, 3, 4\}$ and $PN_{4OUT}(Ai) > PN_{4IN}(Ai)$, $i \in \{5, 6, 7, 8\}$. Therefore, the rapid growth of the OUT part within wild ginseng slows down, as does the accumulation of COCCs; moreover, the accumulation of other secondary metabolites might also slow down. In this time, the degree of COCC accumulation in the IN part catches up to that of the OUT part, and it transcends the volume percentage value of the OUT part, e.g., $PV_{4OUT}(Ai) \approx PV_{4IN}(Ai)$, $i \in \{1, 2, 3, 4\}$ and $PV_{4OUT}(Ai) < PV_{4IN}(Ai)$, $i \in \{5, 6, 7, 8\}$. The above results provide evidence to deduce the growth of the CS structure and the degree of COCC accumulation. As the CS

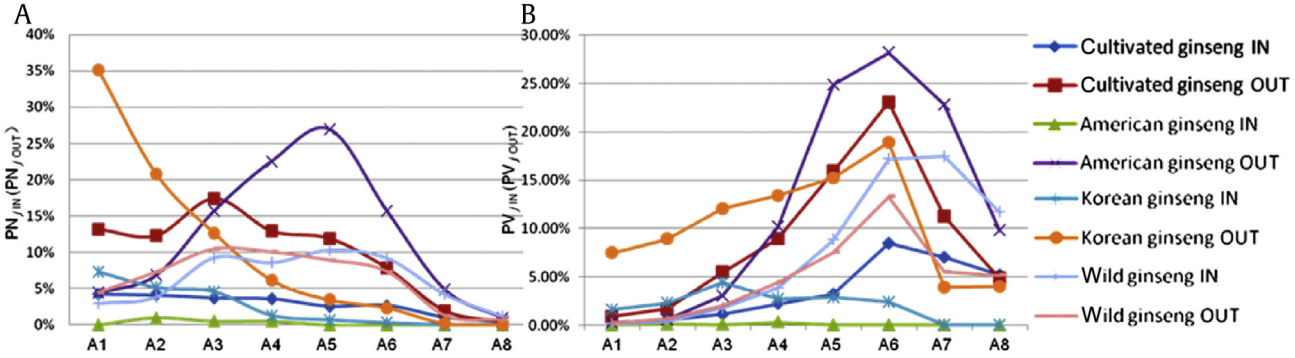

Fig. 6. Percentage of the COCC distribution for the IN and OUT parts across volume ranges of A*i*. (A) The number percentages PN*j*IN(A*i*) and PN*j*OUT (A*i*). (B) The volume percentages PV*j*IN(A*i*) and PV*j*OUT(A*i*). COCC, calcium oxalate cluster crystal.

of ginseng grows in two directions, we can estimate that the growth span of the OUT part was greater than that of the IN part because of the degree of COCC accumulation, provided by the COCC number percentage value (Fig. 6A) and the COCC volume percentage value (Fig. 6B).

In summary, our XPCMT study combined with the phase-retrieval method clearly revealed the microstructures of ginseng. This quantitative imaging and analysis method effectively identified the microstructure of ginseng root. The current work focused on obtaining quantitative information, especially with regard to the important secondary metabolites COCCs in ginseng tissues. We demonstrated that XPCMT successfully performs 3D quantitative imaging and statistical analyses of the COCC distribution. Four types of ginseng were compared: cultivated ginseng, American ginseng, Korean ginseng, and wild ginseng. According to the results regarding the number of COCCs and the volume curves, we can deduce COCC accumulation conditions. Identification information was provided to distinguish between the curves of cultivated ginseng and American ginseng (which are different species), cultivated ginseng and Korean ginseng (which have different growth areas), and cultivated ginseng and wild ginseng (which differ in age) .

4. Conclusions

In conclusion, this study is the first to provide evidence of the distribution characteristics of COCCs to identify four types of ginseng. We demonstrated a new detection method, XPCMT quantitative imaging, which has many advantages; it is noninvasive and nondestructive, and provides *in situ* measurements and 3D quantitative imaging. The results showed that this method could perform feasible comprehensive evaluation of the distribution of COCCs accumulated in ginseng. XPCMT can provide practical information, and it should be applied for the species authentication and age identification of ginseng. This method is also expected to reveal important relationships between COCCs and the occurrence of the effective medicinal components of ginseng. XPCMT quantitative analysis can also be applied to other types of CMMs and even many different kinds of plants having different microstructures and containing different crystalline types, such as calcium oxalate crystals, calcium carbonate crystals, and calcium sulfate crystals.

Conflicts of interest

All authors declare no conflicts of interest.

Acknowledgments

This work was supported by the National Basic Research Program of China (Grant No. 2010CB834301), National Natural Science Foundation of China (No.11475248, 81430087, U1232205), and the CAS-CSIRO Collaborative Research Project (Grant GJHZ1303).

References

[1] Xiao TQ, Bergamaschi A, Dreossi D, Longo R, Olivo A, Pani S, Rigon L, Rokvic T, Venanzi C, Castelli E. Effect of spatial coherence on application of in-line phase contrast imaging to synchrotron radiation mammography. Nucl Instrum Meth A 2005;548:155–62.
[2] Chen RC, Liu P, Xiao TQ, Xu LX. The X-ray Imaging for nondestructive microstructure analysis at SSRF. Adv Mater 2014;26:7688–91.
[3] Ye LL, Xue YL, Tan H, Chen RC, Qi JC, Xiao TQ. X-ray phase contrast micro-tomography and its application in quantitative 3D imaging study of wild ginseng characteristic microstructures. Acta Opt Sin 2013;33:1234002–6.
[4] Ye LL, Xue YL, Ni LH, Tan H, Wang YD, Xiao TQ. Application of X-ray phase contrast micro-tomography to the identification of traditional Chinese medicines. J Instrum 2013;8. http://dx.doi.org/10.1088/1748-0221/1088/1007/C07006.
[5] Li WK, Gu CG, Zhang HJ, Awang DVC, Fitzloff JF, Fong HH, van Breemen RB. Use of high-performance liquid chromatography-tandem mass spectrometry to distinguish *Panax ginseng* C. A. Meyer (Asian Ginseng) and *Panax quinquefolius* L. (North American Ginseng). Anal Chem 2000;72:5417–22.
[6] Liu JH, Burdette JE, Xu HY, Gu CG, van Breemen RB, Bhat KP, Booth N, Constantinou AI, Pezzuto JM, Fong HH, et al. Evaluation of estrogenic activity of plant extracts for the potential treatment of menopausal symptoms. J Agric Food Chem 2001;49:2472–9.
[7] Christensen LP. Ginsenosides chemistry, biosynthesis, analysis and potential health effects. Adv Food Nutr Res 2009;55:1–99.
[8] Attele AS, Wu JA, Yuan CS. Ginseng pharmacology: multiple constituents and multiple actions. Biochem Pharmacol 1999;58:1685–93.
[9] Fournier AR, Proctor JT, Gauthier L, Khanizadeh S, Belanger A, Gosselin A, Dorais M. Understory light and root ginsenosides in forest-grown *Panax quinquefolius*. Phytochemistry 2003;63:777–82.
[10] Konsler TR, Zito SW, Shelton JE, Staba EJ. Lime and phosphorus effects on American ginseng: II. Root and leaf ginsenoside content and their relationship. J Am Soc Hort Sci 1990;115:575–80.
[11] Jackson C, Dini JP, Lavandier C, Faulkner H, Rupasinghe HP, Proctor JT. Ginsenoside content of North American ginseng (*Panax quinquefolius* L. Araliaceae) in relation to plant development and growing locations. J Ginseng Res 2003;27:135–40.
[12] Reynolds LB. Effects of harvest date on some chemical and physical characteristics of American ginseng (*Panax quinquefolius* L.). J Herbs Spices Med Plants 1998;6:63–9.
[13] Reynolds LB. Effects of drying on chemical and physical characteristics of American ginseng (*Panax quinquefolius* L.). J Herbs Spices Med Plants 1998;6:9–21.
[14] Zhang YC, Li G, Jiang C, Yang B, Yang HJ, Xu HY, Huang LQ. Tissue-specific distribution of ginsenosides in different aged ginseng and antioxidant activity of ginseng leaf. Molecules 2014;19:17381–99.
[15] Shi W, Wang YT, Li J, Zhang HQ, Ding L. Investigation of ginsenosides in different parts and ages of *Panax ginseng*. Food Chem 2007;102:664–8.
[16] Zhan DQ, Zhang XM, Sun SQ. Wavelet-transform based identification of ginseng of different ages using two-dimensional infrared correlation spectroscopy. Spectrosc Spect Anal 2007;27:1497–501.
[17] Kim N, Kim K, Choi BY, Lee DH, Shin YS, Bang KH, Cha SW, Lee JW, Choi HK, Jang DS, et al. Metabolomic approach for age discrimination of *Panax ginseng* using UPLC-Q-TOF MS. J Agric Food Chem 2011;59:10435–41.
[18] Zhao ZZ. An illustrated microscopic identification of Chinese materia medica. Shenyang: Liaoning Science and Technology Publishing House; 2005.
[19] Kang TG. Authentication of Chinese medicinal material monographs. Beijing: China Press of Traditional Chinese Medicine; 2007.
[20] Clarke LP, Velthuizen RP, Camacho MA, Heine JJ, Vaidyanathan M, Hall LO, Thatcher RW, Silbiger ML. MRI segmentation: methods and applications. Magn Reson Imaging 1995;13:343–68.
[21] Jung IC, Jeong IS, Kim CS. Distinction of internal tissue of raw ginseng root using a computed tomography scanner. J Ginseng Res 2012;36:469–76.
[22] Yuan CS, Wang CZ, Wicks SM, Qi LW. Chemical and pharmacological studies of saponins with a focus on American ginseng. J Ginseng Res 2010;34:160–7.
[23] Wilkins SW, Gureyev TE, Gao D, Pogany A, Stevenson AW. Phase-contrast imaging using polychromatic hard X-rays. Nature 1996;384:335–8.
[24] Fitzgerald R. Phase-sensitive x-ray imaging. Phys Today 2000;53:23–6.
[25] Smith SY, Smith, Collinson ME, Rudall PJ, Simpson DA, Marone F, Stampanoni M. Virtual taphonomy using synchrotron tomographic microscopy reveals cryptic features and internal structure of modern and fossil plants. PNAS 2009;106:12013–8.
[26] Heeraman DA, Hopmans JW, Clausnitzer V. Three dimensional imaging of plant roots *in situ* with X-ray computed tomography. Plant Soil 1997;189:167–79.
[27] Stuppy WH, Maisano JA, Colbert MW, Rudall PJ, Rowe TB. Three-dimensional analysis of plant structure using high-resolution X-ray computed tomography. Trends Plant Sci 2003;8:2–6.
[28] Kim SA, Punshon T, Lanzirotti A, Li LT, Alonso JM, Ecker JR, Kaplan J, Guerinot ML. Localization of iron in *Arabidopsis* seed requires the vacuolar membrane transporter VIT1. Science 2006;314:1295–8.
[29] Xue YL, Xiao TQ, Du GH, Liu LX, Hu W, Xu HJ. Microscopic identification of *Panax quinquefolius* and *Panax ginseng* by X-ray phase contrast imaging. Acta Opt Sin 2008;28:1828–32.
[30] Wei X, Xiao TQ, Liu LX, Du GH, Chen M, Luo YY, Xu HJ. Application of x-ray phase contrast imaging to microscopic identification of Chinese medicines. Phys Med Biol 2005;50:4277–86.
[31] Xie HL, Deng B, Du GH, Fu YN, Chen RC, Zhou GZ, Ren YQ, Wang YD, Xue YL, Peng GY, et al. Latest advances of X-ray imaging and biomedical application beamline at SSRF. Nucl Sci Tech 2015;26:020102–16.
[32] Nugent KA, Gureyev TE, Cookson DF, Paganin D, Barnea Z. Quantitative phase imaging using hard X-rays. Phys Rev Lett 1996;77:2961–4.
[33] Chen RC, Xie HL, Rigon L, Longo R, Castelli E, Xiao TQ. Phase retrieval in quantitative X-ray microtomography with a single sample-to-detector distance. Opt Lett 2011;36:1719–21.